

Landslide Susceptibility Analysis Based on Three Different Triggering Events and Result Comparison

Chyi-Tyi Lee¹, C.C Huang², C.F. Lee², K.L. Pan³, M.L. Lin⁴
C.W. Liao⁵, P.S. Lin⁵, Y.S. Lin¹, C.W. Chang¹

¹Institute of Applied Geology, National Central University,

²Central Geological Survey, Ministry of Economic Affairs,

³Institute of Applied Geology, National Central University,

⁴Department of Civil Engineering, National Taiwan University,

⁵Institute of Geophysics, National Central University,

ABSTRACT

This study utilizes a geographic information system and a statistical method to integrate geomorphic, geologic and other relevant data, to analyze the basic properties contributing to each landslide potential factor and the triggering factor. The statistical method was used to clarify the correlation of each factor to actual landslides, and to realize the independency of those factors. Several important factors were then selected for further analysis. Rating was done for each selected factor, and the weighting between the factors was determined by using discriminant analysis. Landslide susceptibility analyses were actually performed at a test site in Central Taiwan, at Kuohsing, and susceptibility maps for the test site were made.

Three different triggering events were adopted in the study including two typhoon events and the Chi-Chi earthquake event. Landslides induced by each event were extracted from SPOT imageries and were used in individual analysis. Three landslide susceptibility maps with different trigger factors were made and then were checked against actual landslides associated with the event, so that the probability of landslide occurrence within each susceptibility interval was revealed. As well, three landslide susceptibility maps without trigger factors were also made and compared to each other. They showed similar patterns and values. They may be utilized to prepare a basic landslide susceptibility map of a region which may be used to predict landslide probability due to a triggering event of similar magnitude in this or neighboring regions.

KEYWORD: landslide, landslide susceptibility,

multivariate analysis, discriminant analysis

INTRODUCTION

Regional landslide evaluation and mapping have been pursued by many research institutions and government agencies for a long time. Many different methods and techniques for assessing landslide hazards have been proposed and/or tested. In the early stages, semi-quantitative ratings and the expert weighting method were used (e.g., Carrara and Merenda, 1974; Meneroud and Calvino, 1976; Kienholz, 1977; Malgot and Mahr, 1979; Chang, 1980; Ives and Messerli, 1981; Varnes, 1984; Chen et al., 1985). In the past couple of decades, quantitative approaches using multivariate statistical method have been the trend for the landslide susceptibility studies (e.g., Neuland, 1976; Kobashi and Suzuki, 1988; Gao and Lo, 1991; Koukis, 1991; Carrara et al., 1992; Hearn, 1995; Lee and Min, 2001; Dai and Lee, 2003). Quantitative approaches using the infinite slope analysis method and/or the Newmark displacement method have also been an active branch of landslide susceptibility studies, especially when landslides triggered by earthquakes or heavy rainfall are considered (e.g., Keefer, 1984, 2000; Pearce et al., 1985; Harp et al., 1995; Fukuoka, et al., 1997; Jibson, 1998; Allen, et al., 1998; Polemic and Sdao, 1999; and Jibson et al., 2000). The application of neural networks to landslide susceptibility studies has also been recently attempted by some researchers (Lin, 2003, Lee et al., 2004).

Landslides are a recurrent problem throughout the hilly and mountainous terrain of Taiwan, and cause extensive damage to property and even loss of life. This type of hazard has been particularly great in recent years especially after typhoon Herb (1996),

typhoon Toraji (2001) and the Chi-Chi earthquake (1999). In this study, multivariate statistics was used in the analysis of data, and landslides triggered by an events was selected for training of a susceptibility model. A Geographic Information System (GIS) was used as the basic analysis tool for special data management and manipulation.

This study originated from the necessity of investigating the landslides in Taiwan encouraged by the Central Geological Survey of Taiwan. The aim is to produce a set of 1 to 25 thousand scaled landslide susceptibility maps of Taiwan in the near future. Therefore, we need to make a comprehensive plan and select a typical area to test our hypothesis, method and procedure. Kuohsing, in Central Taiwan, is located in a typical region damaged by the three abovementioned events, and thus was selected as the test site (Fig. 1). The analysis method must be objective and simple, so that it can meet the needs of future work that is to apply the test results to the whole of Taiwan. Discriminant analysis of multivariate statistics was selected as analytical method to determine the weighting of the factors, and the summation of the weighted factors was used to landslide susceptibility mapping. The difference between this study and other studies is that single event data is used for analysis and to compare the results among events. We attempted to produce a basic landslide susceptibility map of one region that would have the potential to be used to predict landslide probability after a triggering event of a similar magnitude, in this or neighboring regions.

PROCEDURE

The landslide susceptibility analysis technique is still being developed. The methodology and procedure may be problem oriented and are highly dependent on data availability. There is no worldwide agreement about this technique. We must therefore adopt a proper methodology and working procedure, according to our intensive paper review and based on our previous experiences, so that the study in the test area could be successful, as well as have prospects for future work. The working procedure for this study is shown in Fig. 2.

BASIC DATA CORRECTION

Data correction was basically based on: a 40m x 40m grid digital terrain model (DTM), SPOT imageries, aerial photographs, 1/50,000 geologic maps of the study area, hourly rainfall records and strong-motion earthquake records of the triggering event of interest. The three triggering events selected were typhoon Herb, typhoon Toraji and the Chi-Chi earthquake. SPOT imageries from 6 different times before and after of the 3 events were selected. They are listed in Table 1. There were both multispectral (XS) and panchromatic (PAN) images for each time, which were used to produce a high resolution false color composite by a fusing technique, for easy recognition of landslides on the image. Stereo-paired aerial photographs were used for the purpose of double checking of landslide locations digitized from the SPOT images.

ESTABLISHMENT OF LANDSLIDE INVENTORY

The location of landslides induced by a typhoon or an earthquake event were first interpreted from SPOT image after each special event, and then checked by examining rectified aerial photographs in GIS. Most misinterpretations of man-made feature or cultivated lands would be recognized on this high resolution image. Some difficult points were further checked by examining stereo-paired aerial photographs under a stereoscope. Landslide deposits could be interpreted from overlapping the analyzed landslide layer and the 1/5,000 scaled topographic contour map and further clarified by the stereo-paired aerial photo technique. Those deposited areas were removed from the landslide group to form the landslide inventory.

SPOT image interpretation was done by Pan et al. (2004, in the same proceedings). The event-induced landslides were mainly interpreted by tone, shape, and association. The final event-induced landslide inventory was compared and further checked against the pre-event landslide inventory, to make sure there were no pre-event landslides included. Fig. 3 demonstrates the comparison and check of event-induced landslides against pre-event landslides.

DETERMINATION OF A HOMOGENEOUS

AREA AND TERRAIN UNITS

The weighting of landslide factors is dependent on local features. There would not be a set of common weightings which could be applied everywhere. The distribution of landslide potential factors may have regional variations, especially from terrain to terrain (Lin and Lee, 2003). Therefore, we need to classify terrain into units before the susceptibility analysis. We have made an unsupervised classification of many geomorphic and geologic factors and classifying them into 13 terrain units. The methodology used is the iterative self-organizing data analysis technique (ISODATA), which aims at finding the minimum difference within a cluster and the minimum similarity among clusters. The results are shown in Fig. 1.

In the present study area, there are 3 different terrain units, namely, hilly terrain, mountainous terrain and slate terrain. In the actual study, the latter two units were combined, because in this area slate terrain is also part of mountain area geomorphologically. The difference between the two units may have been reflected in the lithology factor.

PROCESSING AND RATING OF POTENTIAL FACTORS

More than fifty different factors have been used in Taiwan and worldwide for landslide susceptibility analysis (Lin, 2003). Of these, we selected 15 frequently used factors, as the first step, by considering whether a factor is substantial and assessable. The factors are the lithology, slope, slope aspect, terrain roughness, slope roughness, slope curvature (profile curvature, plane curvature, tangential curvature, total curvature), slope height, total slope height, distance to a road, distance to a fault, distance to river head, distance to a river bend, NDVI (Normalized Difference Vegetation Index), and the two trigger factors – earthquake intensity and rainfall. All these selected factors were processed and the frequency distribution of the landslide group and the non-landslide group, in hilly terrain and mountainous terrain, was plotted and visually inspected. A factor having more distinct differences in distribution between the landslide group and the non-landslide group is

more important for landslide occurrence. Accordingly, from the thirteen potential factors, 6 were extracted for the actual earthquake induced landslide susceptibility analysis, and 8 potential factors were selected for typhoon induced landslide susceptibility analysis. The frequency distribution of the Chi-Chi landslide group and the non-landslide group of 4 typical factors are shown in Fig. 4 as an example.

The internal rating of a factor was according to the landslide ratio of an event. The rated values were then normalized in the range of 0 to 1. The relation between the landslide ratio and a factor is also shown in Fig. 4.

PROCESSING AND RATING THE TRIGGER FACTORS

Strong-motion records of the main shock of the Chi-Chi earthquake, and 6 major aftershocks, were corrected and processed for Arias intensity (I_a) at each station. These were then used to interpolate by the Kriging method at each grid point for each earthquake. Because the landslide inventory of the Chi-Chi event was interpreted from the SPOT image 6 days after the main shock, the 6 major aftershocks that occurred within this time span should be taken into consideration. We checked each grid point to find the maximum intensity among the 7 earthquakes and adopted the maximum value as the intensity that triggered the landslides present on the SPOT image. The Isoleths map of I_a is shown in Fig. 5a. The frequency distribution and landslide ratio are shown in Figs. 5b and 5c. We further consider the topographic effects of the earthquake intensity. We found that the factor of height relative to riverbed (Fig. 5d) was good for making corrections, and finally adopted an experience equation proposed by Lin and Lee (2003):

$$I_a' = I_a F \quad (1)$$

$$F = \sqrt{H / 93.799 + 0.287} + 0.464 \quad (2)$$

where I_a is corrected to be I_a' by the amplification factor F , and H is the height relative to riverbed. The I_a' adopted in the analysis is shown in Fig. 5g. The frequency distribution of the landslide and non-landslide groups as well as landslide ratio for I_a' , the height relative to riverbed, and the I_a , are shown in Figs. 5h and 5i.

For the Herb and Toraji typhoon events, the

hourly rainfall records were corrected and processed to find the hourly maximum rainfall (rainfall intensity) and total rainfall of the events. These were then interpolated at each grid point, by the Kriging method, for each event. Fig. 6 is an example of the rainfall factor from typhoon Toraji.

DISCRIMINANT ANALYSIS AND WEIGHT DETERMINATION

When applying the multivariate method in landslide susceptibility analysis, we aimed at finding the best linear equation to calculate the susceptibility value λ as follows:

$$\lambda_i = \sum_j w_j F_{ij} \quad (3)$$

where λ_i is susceptibility value at the i th point; w_j is the weight of the j th factor; F_{ij} is rating of the j th factor at the i th point. Data set F_i may be expressed as

$$\mathbf{F}_i = \langle F_{i1}, F_{i2}, F_{i3}, \dots, F_{ij} \rangle \quad (4)$$

In discriminant analysis, the data should be divided into landslide and non-landslide groups; these data sets are named **A** and **B**, respectively. Then we calculate the pooled variance and covariance matrix **S**, and the difference between the two multivariate means to form a vector **D**. They are described as

$$\mathbf{D} = \bar{\mathbf{A}} - \bar{\mathbf{B}} \quad (5)$$

where $\bar{\mathbf{A}}$ is the multivariate mean for group A, $\bar{\mathbf{B}}$ is the multivariate mean for group B, and

$$\mathbf{S} = \frac{\mathbf{S}_A + \mathbf{S}_B}{n_a + n_b - 2} \quad (6)$$

where \mathbf{S}_A is the variance and covariance matrix of group A, and \mathbf{S}_B is the variance and covariance matrix of group B; n_a is the number of data in group A, and n_b is the number of data in group B. Solving the following equation, the weighting vector **W** can be obtained:

$$\mathbf{S}\mathbf{W} = \mathbf{D} \quad (7)$$

so that,

$$\mathbf{W} = \mathbf{S}^{-1}\mathbf{D} \quad (8)$$

The weighting vector **W** may also be expressed as

$$\mathbf{W} = \langle w_1, w_2, w_3, \dots, w_j \rangle \quad (9)$$

In landslide susceptibility analysis, we should consider unbiasedness, so that the total weight be equal to unity, i.e.:

$$\sum_i w_i = 1 \quad (10)$$

Because the factors have been all previously normalized, the susceptibility value λ should also be between 0 and 1. The discriminant index R_0 is defined as

$$R_0 = \sum_j w_j X_j \quad (11)$$

where

$$X_j = \frac{\bar{A}_j - \bar{B}_j}{2} \quad (12)$$

When λ_i is greater than R_0 , the point may be classified into the landslide class, or may be predicted as landslide, and thus we say this point belongs to a high susceptibility class.

RESULT MAPPING AND EVALUATION

THE CHI-CHI EARTHQUAKE EVENT

The test site was divided into two terrain units for analysis. The linear equations for discriminant analysis are as follows:

Hilly terrain (west of the Hsuangtung fault):

$$\lambda_1 = .047F_1 + .334F_2 + .030F_3 + .061F_4 + .018F_5 + .044F_6 + .465F_7 \quad (13)$$

Mountainous terrain (east of the Hsuangtung fault):

$$\lambda_2 = .019F_1 + .413F_2 + .025F_3 + .205F_4 + .051F_5 + .022F_6 + .265F_7 \quad (14)$$

where F_1 is the lithology, F_2 is slope, F_3 is slope aspect, F_4 is terrain roughness, F_5 is slope roughness, F_6 is total curvature, and F_7 is the Arias intensity. The discriminant index is as follows:

Hilly terrain (west of the Hsuangtung fault):

$$R_{01} = 0.250 \quad (15)$$

Mountainous terrain (east of the Hsuangtung fault):

$$R_{02} = 0.226 \quad (16)$$

We further defined the boundary between moderately high and moderate susceptibility as being half of R_0 , we defined the boundary between moderately and moderately low susceptibility as a quarter of R_0 , and defined the boundary of moderately low and low susceptibility as half of a quarter of R_0 . According to these definitions, we

drew the landslide susceptibility map in Fig. 7, the relations between the landslide ratio and λ_i are shown in Fig. 8, for realizing the probability of a landslide in each susceptibility interval. The landslide group data and non-landslide group data were projected onto a discriminant function line and are also shown in Fig. 8 to realize the goodness of the results. If we compare the actual landslides with the susceptibility map, we may find that 55% of the landslides were located at high susceptibility grids, 81 % above the moderately high grids, and 94% above the moderate grids (see Table 2).

THE TYPHOON TORAJI EVENT

The test site was divided into two terrain units for analysis. The linear equations for discriminant analysis are as follows:

Hilly terrain (west of the Hsuangtung fault):

$$\lambda_3 = -.019F_1 + .162F_2 + .057F_3 + .479F_4 - .108F_5 + .210F_6 + .090F_7 + .092F_8 + .038F_9 \quad (17)$$

Mountainous terrain (east of the Hsuangtung fault):

$$\lambda_4 = .024F_1 + .287F_2 + .103F_3 + .075F_4 - .014F_5 + .006F_6 + .410F_7 + .005F_8 + .104F_9 \quad (18)$$

Where F_1 is the lithology, F_2 is slope, F_3 is slope aspect, F_4 is terrain roughness, F_5 is slope roughness, F_6 is total curvature, F_7 is NDVI, F_8 is total slope height, and F_9 is the maximum hourly rainfall. The discriminant index is:

Hilly terrain (west of the Hsuangtung fault):

$$R_{04} = 0.289 \quad (19)$$

Mountainous terrain (east of the Hsuangtung fault):

$$R_{04} = 0.319 \quad (20)$$

We further defined the boundary between moderately high and moderate susceptibility as being half of R_0 , we defined the boundary between moderately and moderately low susceptibility as a quarter of R_0 , and defined the boundary of moderately low and low susceptibility as half of a quarter of R_0 . According to these definitions, we drew the landslide susceptibility map in Fig. 9. The relations between the landslide ratio and λ_i are shown in Fig. 10, for realizing probability of a landslide in each susceptibility interval. The landslide group data

and non-landslide group data were projected onto the discriminant function line and are also shown in Fig. 10, to realize the goodness of the results. If we compare the actual landslides with the susceptibility map, we find that 55% of the landslides were located in the high susceptibility grids, 81 % above the moderately high grids, and 94% above the moderate grids (see Table 2).

THE TYPHOON HERB EVENT

The test site was divided into two terrain units for analysis. The linear equations for discriminant analysis are as follows:

Hilly terrain (west of the Hsuangtung fault):

$$\lambda_5 = .038F_1 + .702F_2 + .092F_3 + .040F_4 + .136F_5 - .061F_6 + .025F_7 + .016F_8 + .012F_9 \quad (21)$$

Mountainous terrain (east of the Hsuangtung fault):

$$\lambda_6 = .027F_1 + .411F_2 - .046F_3 + .135F_4 + .084F_5 + .005F_6 + .275F_7 + .036F_8 + .072F_9 \quad (22)$$

Where, F_1 is the lithology, F_2 is slope, F_3 is slope aspect, F_4 is terrain roughness, F_5 is slope roughness, F_6 is total curvature, F_7 is NDVI, F_8 is total slope height, and F_9 is the maximum hourly rainfall. The discriminant index is:

Hilly terrain (west of the Hsuangtung fault):

$$R_{05} = 0.365 \quad (23)$$

Mountainous terrain (east of the Hsuangtung fault):

$$R_{06} = 0.310 \quad (24)$$

We further defined the boundary between moderately high and moderate susceptibility as being half of R_0 , we defined the boundary between moderately and moderately low susceptibility as a quarter of R_0 , and defined the boundary of moderately low and low susceptibility as half of a quarter of R_0 . According to these definitions, we drew the landslide susceptibility map in Fig. 11. The relations between the landslide ratio and λ_i for realizing probability of a landslide in each susceptibility interval are shown in Fig. 12. The landslide group data and non-landslide group data were projected onto the discriminant function line and are also shown in Fig. 12, to realize the goodness of the results. If we compare the actual landslides with the susceptibility map, we can find that 55% of the landslides are located at high susceptibility grids, 81 % above the moderately high grids, and 94% above the moderate grids (see Table 2).

COMPARISON AMONG PRE-EVENT MAPS

In the previous section, we presented three no-trigger-factor susceptibility maps (Figs. 7b, 9b, and 11b). This kind of map may represent pre-event susceptibility. When we visually inspect and compare these maps, we find they show similar values and patterns. High susceptibility areas at some common locations are: (1) the Giogio mountain and Toukeshan, Quaternary molasse conglomerate, (2) the escarpments of the Tahengping mountain ridge, (3) the Shinse terrace scarps, (4) scarps at sides of the Tapingting tableland, and (5) Eocene sandstone terrain in the slate belt.

If we compare those maps by subtracting them from each other, we may examine them more quantitatively. The maps after subtraction are shown in Fig. 13. The results show general agreement between values, with some variation at local points. Figs. 14b, and c show a distinctly low value at the Giogio mountain. This may be due to before the Chi-Chi earthquake, this region being relatively more stable.

If we compare the actual landslides before the event with the pre-event susceptibility maps, we may find that the results are as good as the event results, except for the pre-Chi-Chi event (see Table 2). This may be explained by the origin or the triggering conditions of the pre-event landslides and the event-induced landslides being different. The former is caused by rainfall, and the latter is triggered by earthquake.

DISCUSSION AND CONCLUSION

Landslide susceptibility analysis technique is actively developing, and there is as yet no worldwide agreement regarding the methodology or procedure. This may be problem oriented and is highly dependent on the availability of data. The present study proposed a multivariate statistic approach via discriminant analysis including the trigger factor by a specific earthquake or typhoon event, at a test site at Kuohsing. The high susceptibility results show good agreement with landslides actually induced by individual events. The no-trigger-factor susceptibility maps are also good at predicting the pre-event landslides. These

imply that the present methodology and working procedure are good, and may have potential to be used for the prediction of landslide probability after a triggering event of similar magnitude in this or neighboring regions.

However, this study is only a start, we need to improve the methodology and enhance the data quality, so that the accuracy of the prediction will be increased. Prediction of earthquake-induced landslides by the Newmark displacement method has already been tested and will be presented at the same conference (Liao and Lee, 2004). The prediction of landslides by the application of neural networks has also been done for a similar area in Central Taiwan (Lin, 2003). Testing of the application of logistic regression, at the same place, is still in progress. Neural networks application generally seems to lead to better accuracy of prediction, but the physical meaning of the method is still dimly understood and the procedure is more complicated and time consuming.

The physical meaning of discriminant analysis is clear, but it is not appropriate for all categories of data, like lithology. It is also not good for data that deviated from a normal distribution. These issues need to be improved in the near future. The weights derived from the discriminant analysis are still apparent. They cannot totally reflect the importance of an individual factor, because there still exists some dependency between factors. We need to first search out and find more good factors for analysis, then the exclude some of the dependent factor to get better and more stable result.

In present study, we obtained a rather good result by processing of Arias intensity. However, we believe that if we increase the training area to cover most earthquake-induced landslides, the results would be even better. As to the rainfall factors, we actually did not get a good result, because the training area was too small. This must be improved in a further study.

ACKNOWLEDGEMENTS

This research was supported by the Central Geological Survey, Ministry of Economic Affairs, Taiwan, under the Landslide Research Project. The authors are deeply appreciative to Director C.C. Lin for his concern for this project and for helpful hints. The authors also express their appreciation to several

reviewers of this project for their enthusiastic advice and valuable suggestions.

REFERENCES

- Allen, Clarence R., James N. Brune, Lloyd S. Cluff, Allan G Barrows, Jr. (1998) Evidence for unusually strong near-field ground motion on the hanging wall of the San Fernando fault during the 1971 earthquake, *Seismological Research Letters*, 69(6), 524-531.
- Carrara, A. and Merenda, L. (1974) Methodology for an inventory of slope instability events in Calabria (southern Italy), *Geologia Applicata e Idrogeologica*, 9, 237-255.
- Carrara, A., M. Cardinali, R. Detti, F. Guzzetti (1992) Uncertainty in Assessing Landslide Hazard and Risk, *ITC Journal*, 2, 172-183.
- Chang, S.C. (1980) Investigation and mapping of landuse potential in urban area, *Proceedings of Land Coservation Society of Chunghua*, 11(1), 13-24.
- Chen, C.H. and Kuo-Liang Pan (1985) Environmental geological investigation of slope land in the Taipei City, *MRSO Report*, 229, 385p.
- Dai F.C. and Lee C.F. (2001) Frequency-volume relation and prediction of rainfall-induced landslides, *Engineering Geology*, 59, 253-266.
- Fukuoka, H., Sassa, K., and Scarascia-Mugnozza, G (1997) Distribution of landslides triggered by the 1995 Hyogo-ken Nanbu earthquake and long runout mechanism of the Takarazuka golf course landslide, *J. phys. Earth.*, 83-90.
- Gao, J. and C.P. Lo (1991) GIS Modeling of Influence of Topography and Morphology on Landslide Occurrence in Nelson County, Virginia: *GIS/LIS '91 Proceedings*, 1, 954-963.
- Harp, E.L., Wilsoon, R.C., (1995) Shaking Intensity Thresholds for Rock Falls and Slides : Evidence from 1987 Whittier Narrows and Superstition Hills Earthquake Strong-Motion Records, *Bull. Seis. Soc. Am.*, 85(6), 1739-1757.
- Hearn, G J. (1995) Landslide and erosion hazard mapping at Ok Tedi Cooper Mine, *The Quarterly Journal of Engineering Geology*, 28, 47-60.
- Ives, J.D., and B. Messeri (1981) Mountain Hazards Mapping in Nepal: Introduction to an Applied Mountain Research Project, *Mountain Research and Development*, 1(3-4), 223-230.
- Jibson, R.W., E.L. Harp, and J.A. Michael (1998) A method for producing digital probabilistic seismic landslide hazard maps: an example from the Los Angeles, California Area, *USGS Open-File Rep.* 98-113.
- Jibson, R.W., Harp, E.L., Michael, J.A. (2000) A Method for Producing Digital Probabilistic Seismic Landslide Hazard Maps, *Engineering Geology*, 58, 271-289
- Keefe, D.K. (2000) Statistical Analysis of an Earthquake-Induced Landslide Distribution - the 1989 Loma Prieta, California Event, *Engineering Geology*, 58, 231-249.
- Keefe, D.K., (1984) Rock avalanches caused by earthquakes: source characteristics, *Science*, 223, 1288-1290
- Kienholz, H., (1977) Kombinierte Geomorphologische Gefahrenkarte 1:10,000 von Grindelwald, *Catena*, 3, 265-294.
- Kobashi, S., and M. Suzuki (1988) Hazard Index for the Judgement of Slope Stability in the Rokko Mountain Region, In *Proc., Interpraevent 1988*, Graz, Austria, 1, 223-233.
- Koukis, G and Ziourkas, C. (1991) Slope Instability Phenomena in Greece: A Statistical Analysis, *Bulletin of the International Association of Engineering Geology*, 43, 47-60.
- Lin Po-Shen and Chyi-Tyi Lee (2003) Arias Intensity in landslide susceptibility analysis, *Proceeding of 2003 Annual Meeting of Chinese geophysical Society*, 91-96.
- Lin Yen-Hsiang (2003) Application of neural networks to landslide susceptibility analysis, *M.S. Thesis of Institute of Applied Geology, National Central University*, 81p.
- Lin Shu-Yuan and Chyi-Tyi Lee (2003) Regional variation of landslide potential factors, *Proceeding of 2003 Annual Meeting of Geological Society of China*, p44.
- Malgot, J., and T. Mahr (1979) Engineering Geological Mapping of the West Carpathian Landslide Areas, *Bulletin of the International Association of Engineering Geology*, 19, 116-121.

- Meneroud, J. P., Calvino, A. (1976) Carte ZERMOS, Zones exposees a des Risques lies aux Mouvements du Sol et du Sous-Sol a 1:25,000, Region de la Moyenne Vesubie (Alpes-Maritimes), Bureau de Recherches Geologiques et Minières, Orleans, France, 11p.
- Neuland, H. (1976) A Prediction Model of Landslides, Catena, 3, 215-230.
- Pearce, A. J. and O'Loughlin, C. L. (1985) Landsliding during a M7.7 earthquake: influence of geology and topography, Geology, 13, 855-858.
- Polemic, M. and F. Sdao (1999) The role of rainfall in the landslide hazard: the case of the Avigliano urban area (Southern Apennines, Italy) , Eng. Geol., 53, 297-309.
- Varnes, D.J. (1984) Landslide Hazard Zonation: A Review of Principles and Practice, UNESCO Press, Paris, 63p.

Table 1 SOPT imageries used in the study

Event	Image	Time	Series number	Type
Before Typhoon Herb	1	1996/04/17	G0004681	XS
	2	1996/04/17	G0004683	PAN
After Typhoon Herb	3	1996/11/08	G0009610	XS
	4	1996/11/08	G0005962	PAN
Before Chi-Chi Earthquake	5	1999/04/01	G0012701	XS
	6	1999/04/01	G0013125	PAN
After Chi-Chi Earthquake	7	1999/09/27	G0013087	XS
	8	1999/09/27	G0013091	PAN
Before Typhoon Toraji	9	2001/07/02	G0015182	XS
	10	2001/07/02	G0014757	PAN
After Typhoon Toraji	11	2001/11/10	G0014977	XS
	12	2001/11/10	G0014975	PAN

Table 2 Accurate rates of the 6 landslide susceptibility maps

Event	Accurate rate 1* ¹	Accurate rate 2* ²	Accurate rate 3* ³
Toraji	68.36%	90.12%	97.27%
Pre-Toraji	67.85%	89.75%	96.06%
Chi-Chi	54.66%	80.92%	93.62%
Pre-Chi-Chi	13.18%	28.17%	46.73%
Herb	57.27%	84.60%	94.88%
Pre-Herb	37.31%	85.35%	94.50%

*Note : 1. Percentage of actual landslides belonging to the high susceptibility,
2. Percentage of actual landslides above the moderately high susceptibility,
3. Percentage of actual landslides above the moderate susceptibility.

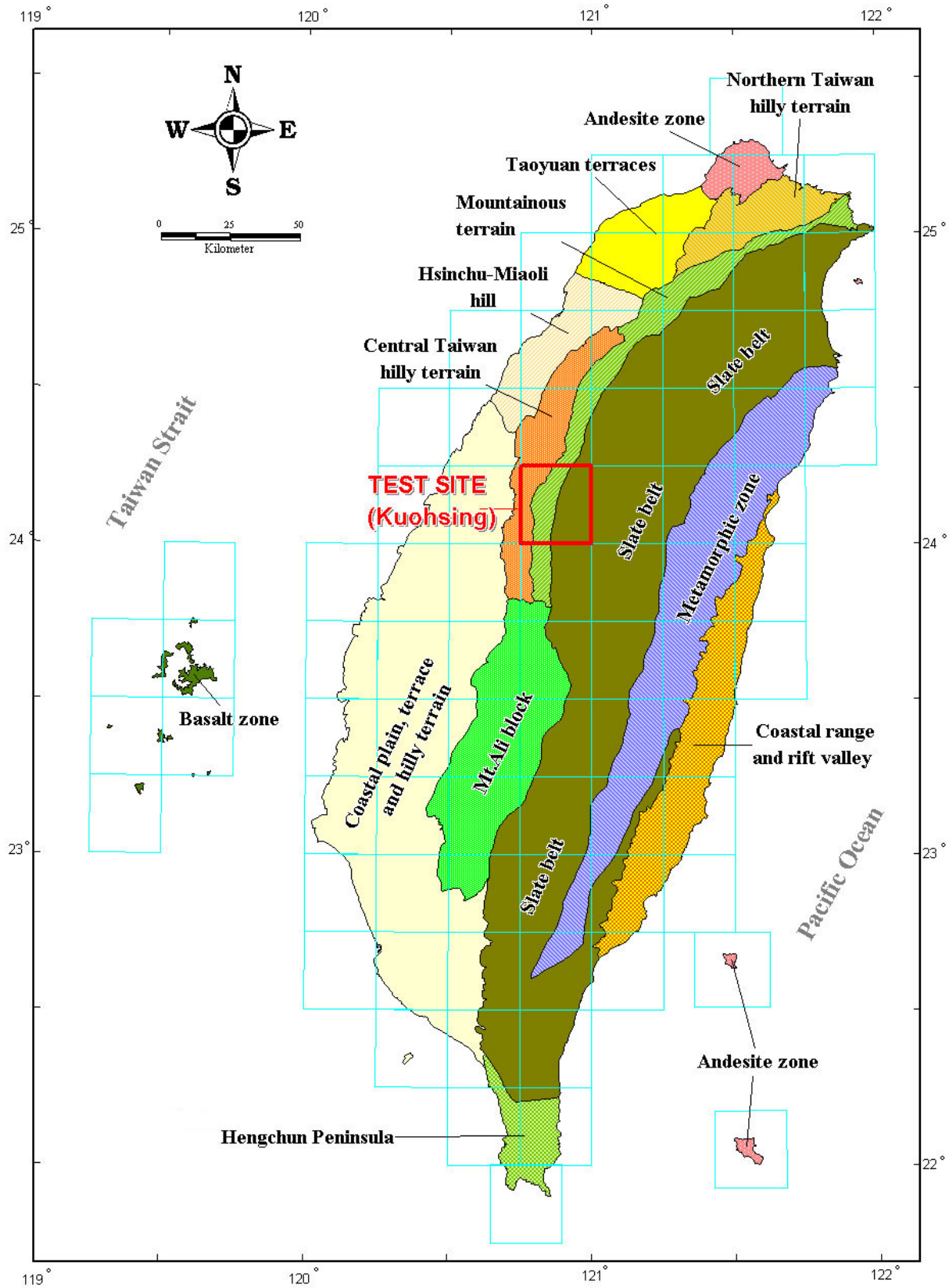


Fig. 1 Test area and terrain units in Taiwan

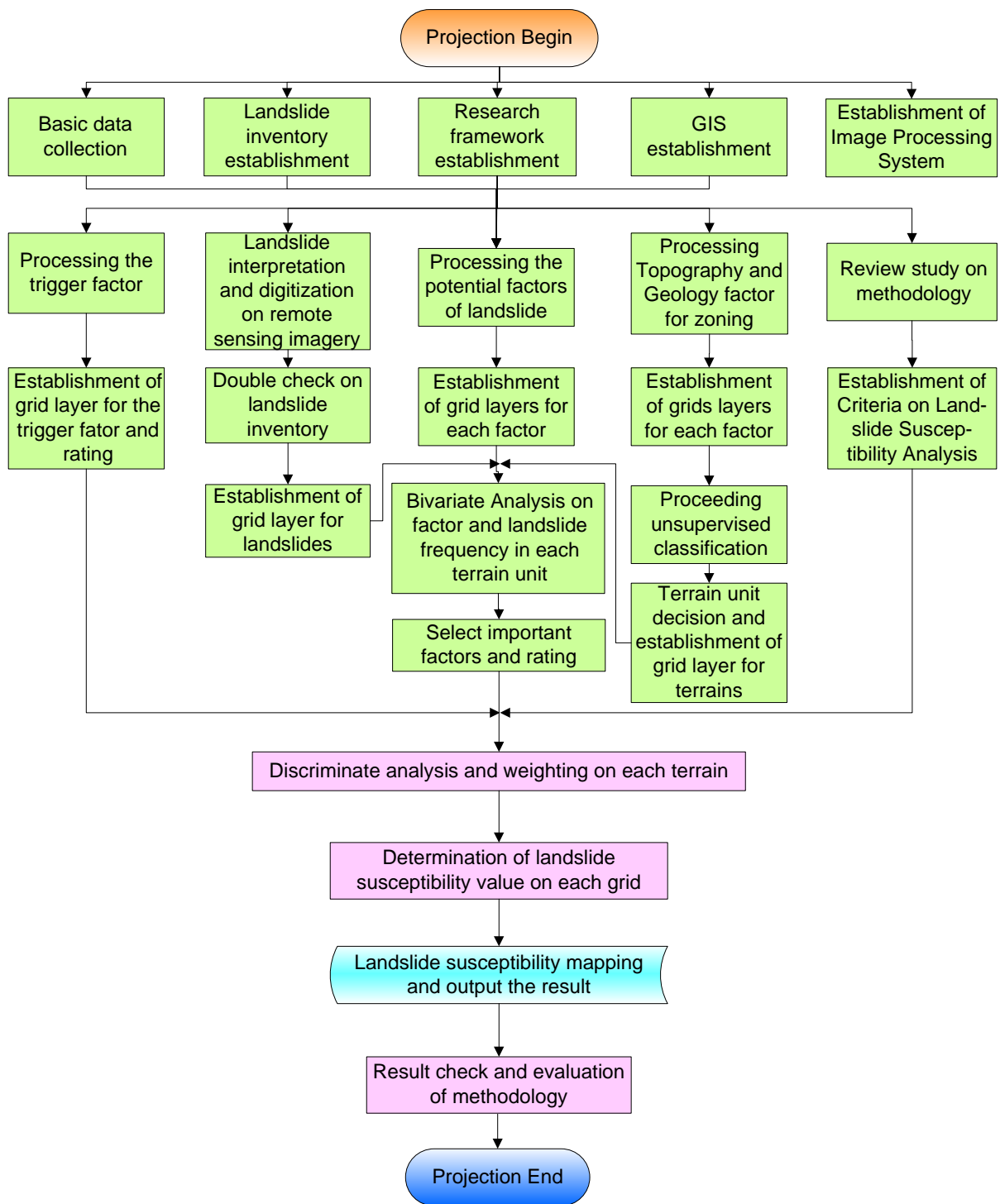


Fig. 2 Working procedure for single-event landslide susceptibility analysis in this study

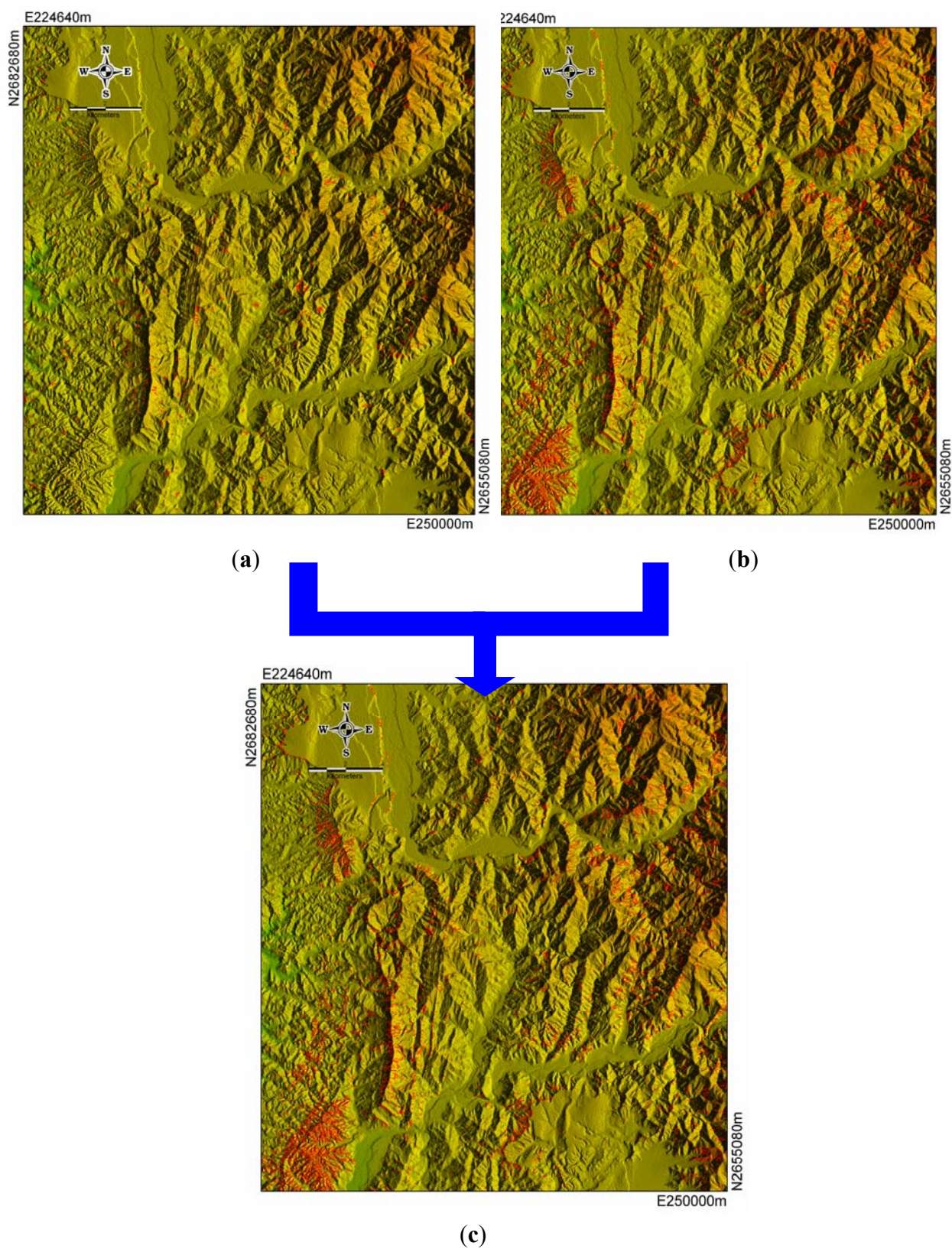


Fig. 3 Comparison and double check of landslides triggered in an event. (a) Landslides before Chi-Chi earthquake, (b) landslides after Chi-Chi earthquake, (c) landslides triggered by the Chi-Chi earthquake.

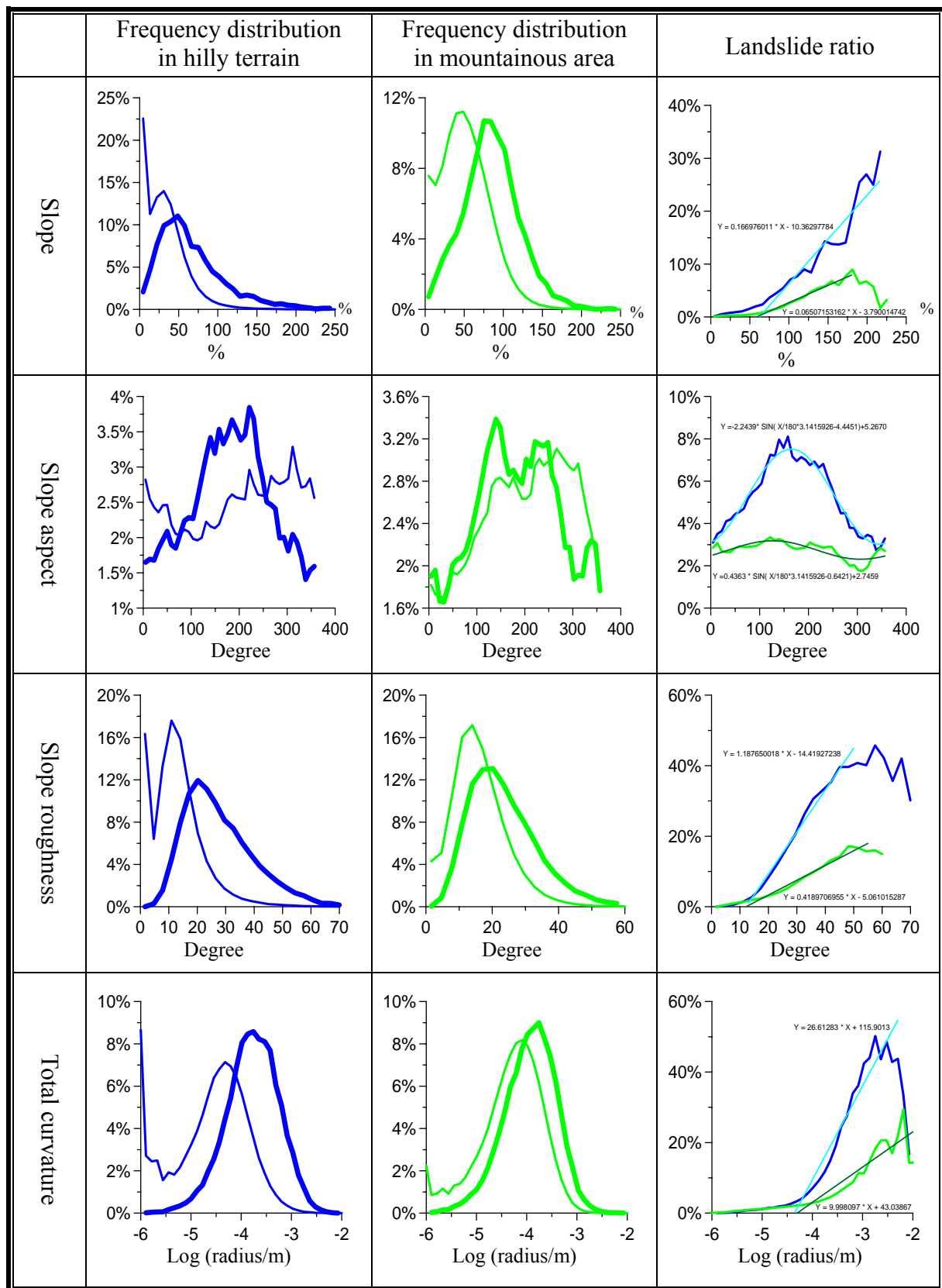


Fig. 4 Bivariate analysis and landslide ratio of typical factors in Chi-Chi earthquake event. Thick line indicates landslide group, thin line indicates non-landslide group, blue color indicates results in hilly terrain, and green color indicates results in mountainous region.

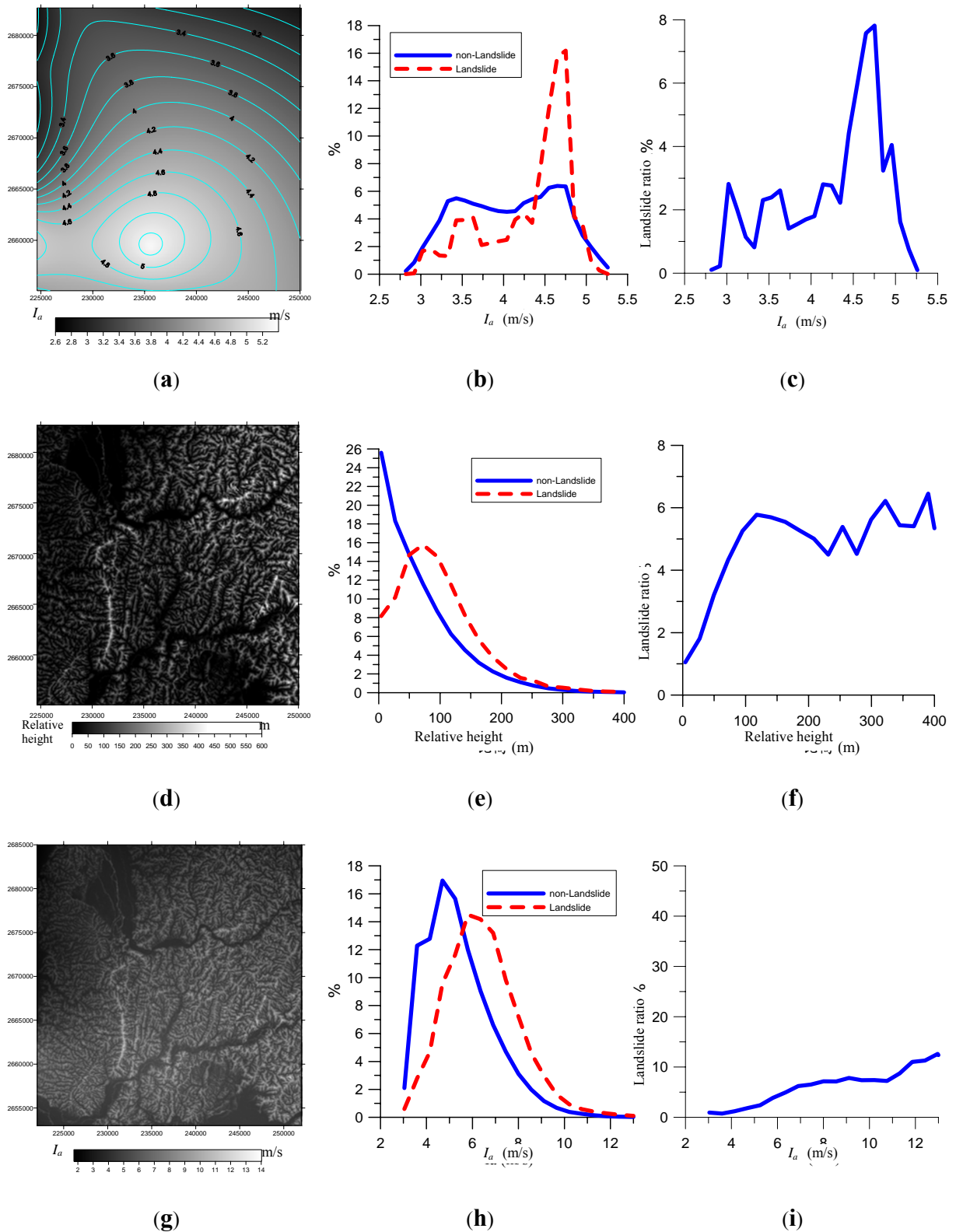


Fig. 5 Arias intensity (I_a) of the Chi-Chi earthquake at test site. (a) I_a , maximum of main shock and aftershocks, (b) statistical plot of I_a maximum, (c) landslide ratio with I_a , (d) height relative to riverbed, (e) statistical plot of height relative to riverbed, (f) landslide ratio with height relative to riverbed, (g) grid map of I_a after correction by relative height, (h) statistical plot of I_a after correction, (i) landslide ratio with I_a after correction.

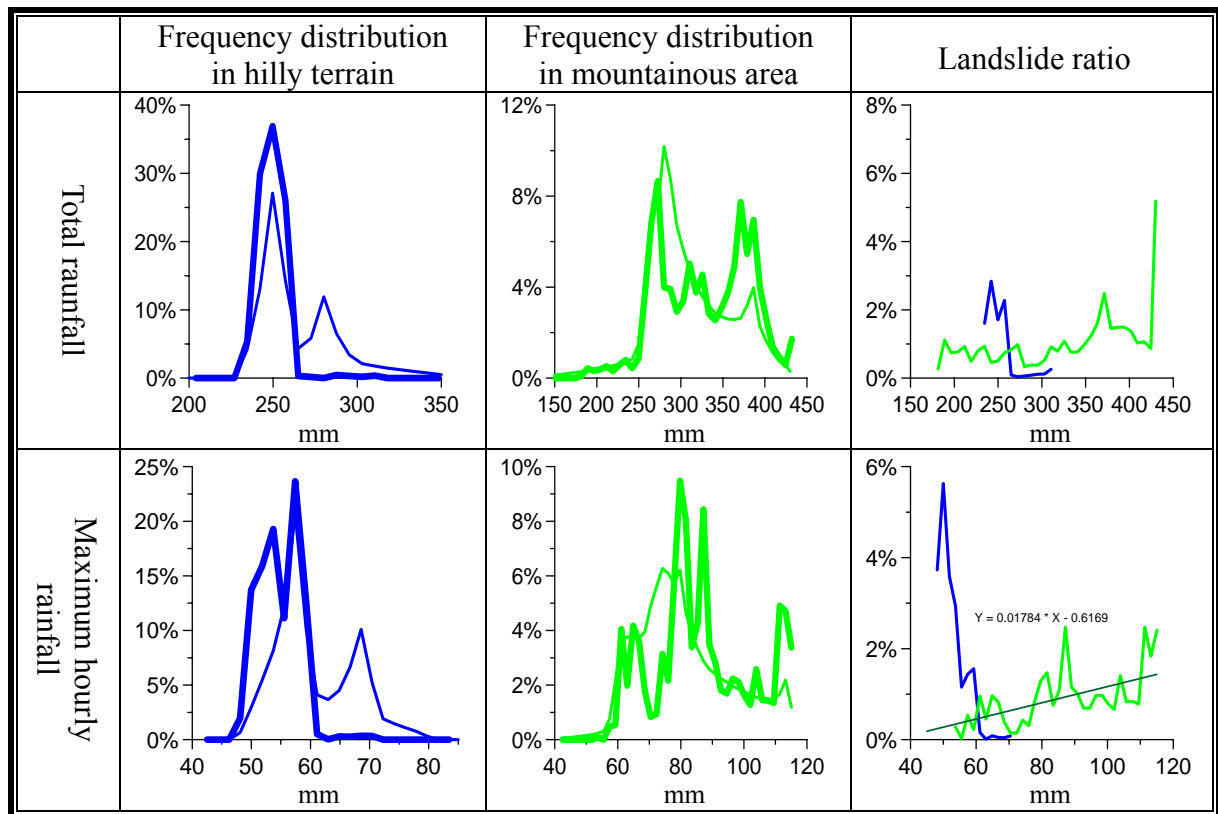
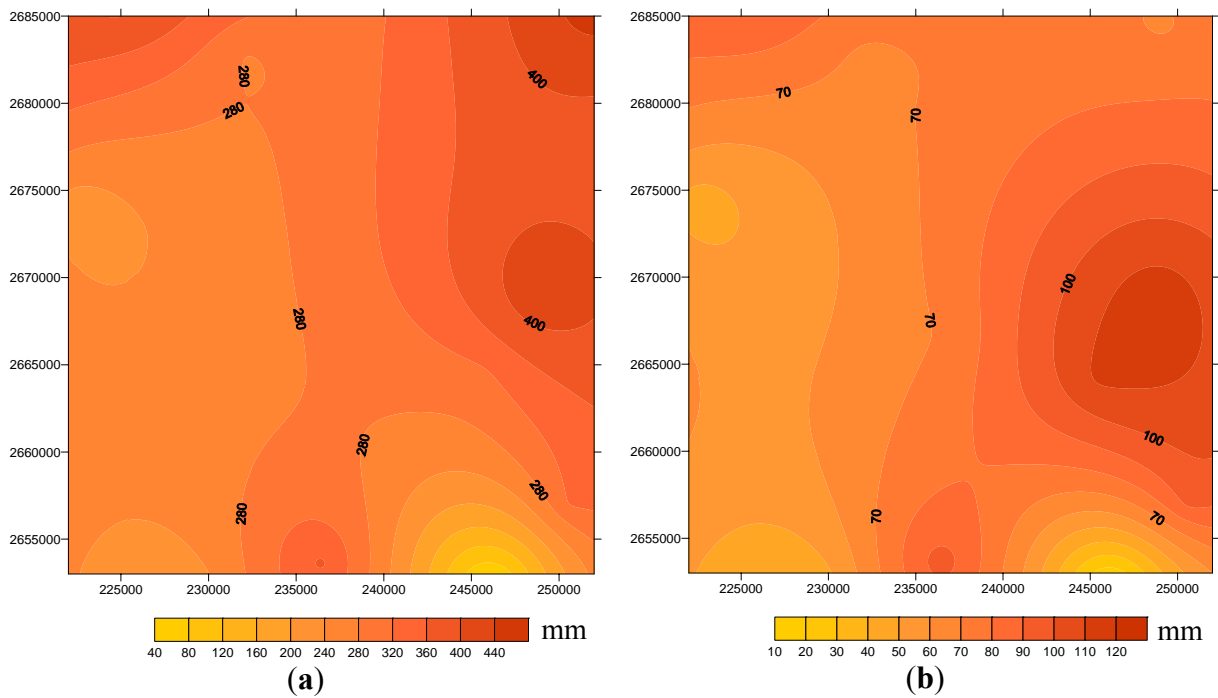


Fig.6 Rainfall of typhoon Toraji at test site. (a) Total rainfall, (b) Maximum hourly rainfall, (c) Bivariate analysis and landslide ratio of total rainfall and maximum hourly rainfall factors. Thick line indicates landslide group, thin line indicates non-landslide group, blue color indicates results in hill terrain, and green color indicates results in high mountain region.

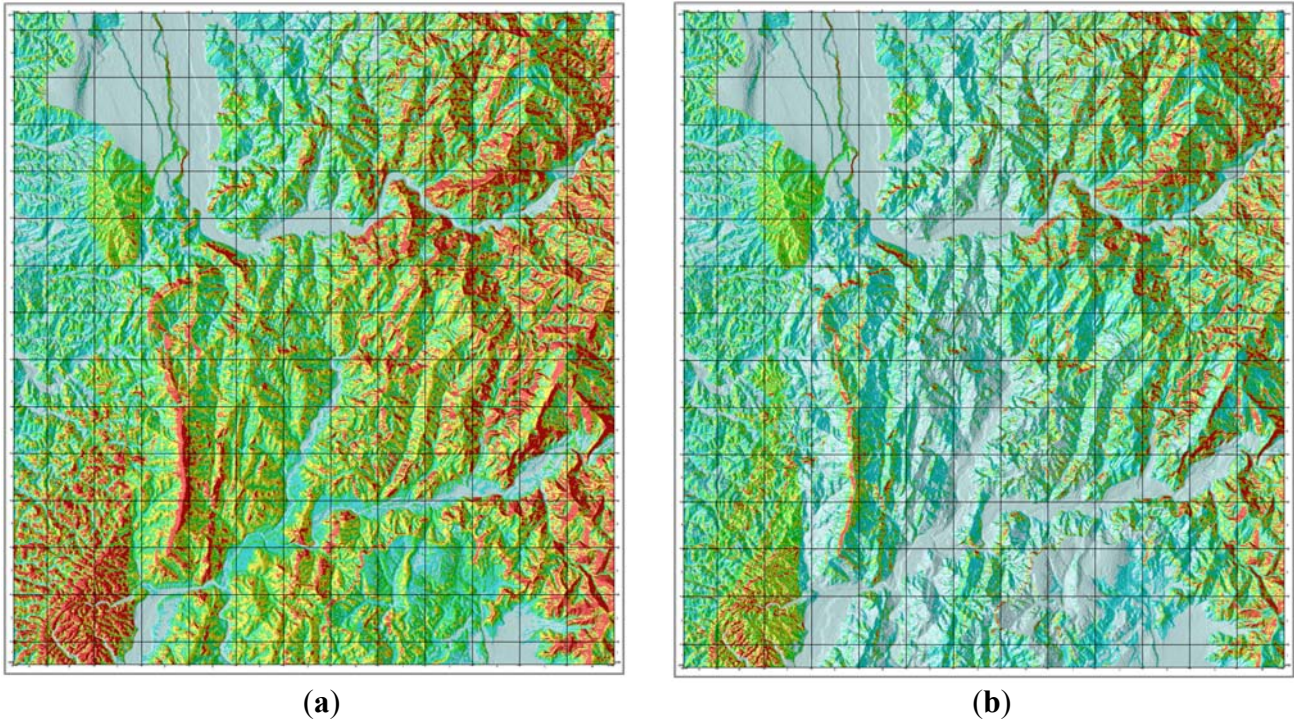


Fig. 7 Landslide susceptibility maps of the Chi-Chi event. Red indicates high susceptibility, yellow moderately high, green moderate. (a) The Chi-Chi event, (b) pre-Chi-Chi event.

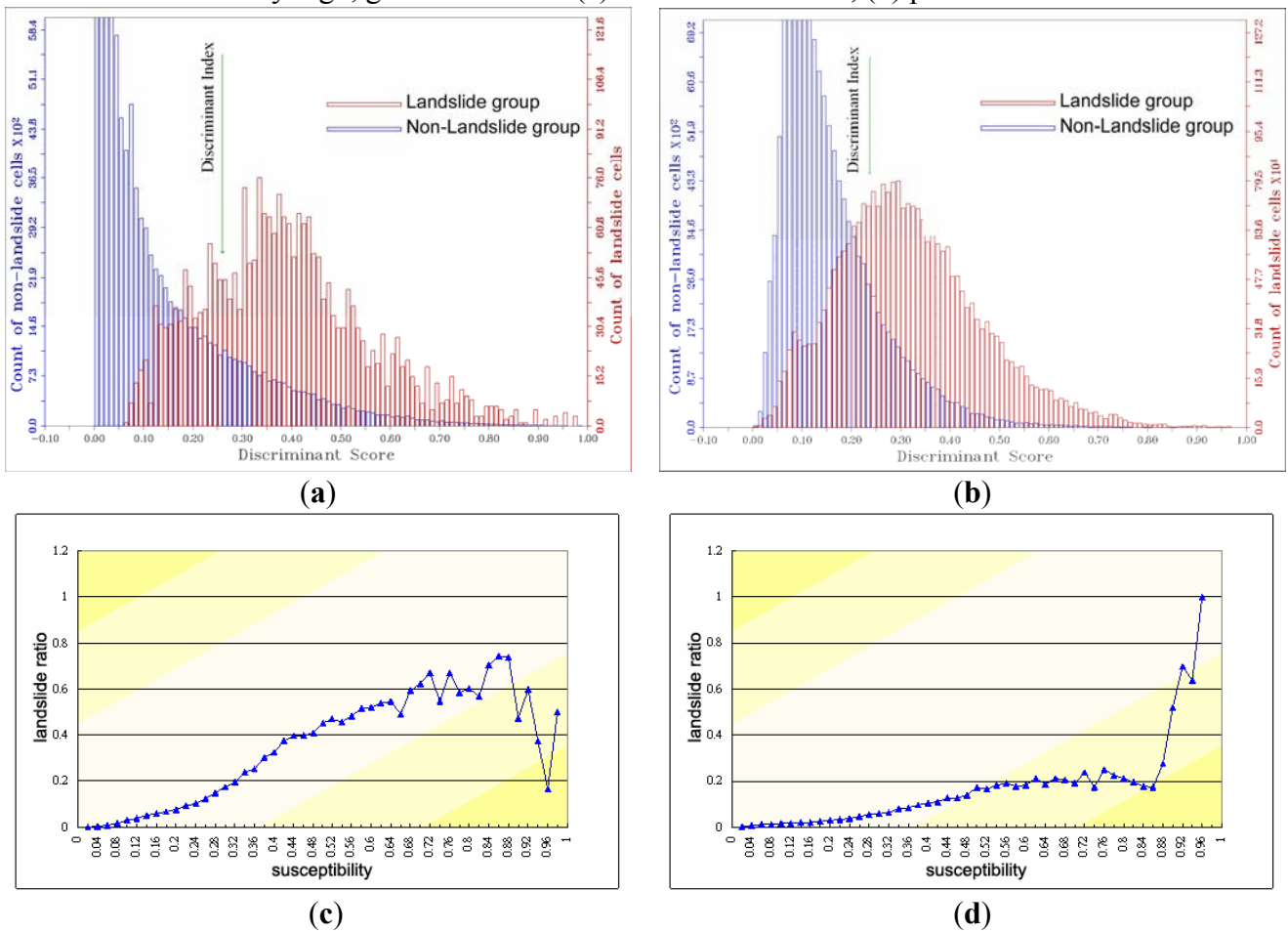


Fig. 8 Frequency distribution of discriminant score in (a) hilly terrain and (b) mountainous terrain, and landslide ratio distribution of susceptibility value in (c) hilly terrain and (d) mountainous terrain.

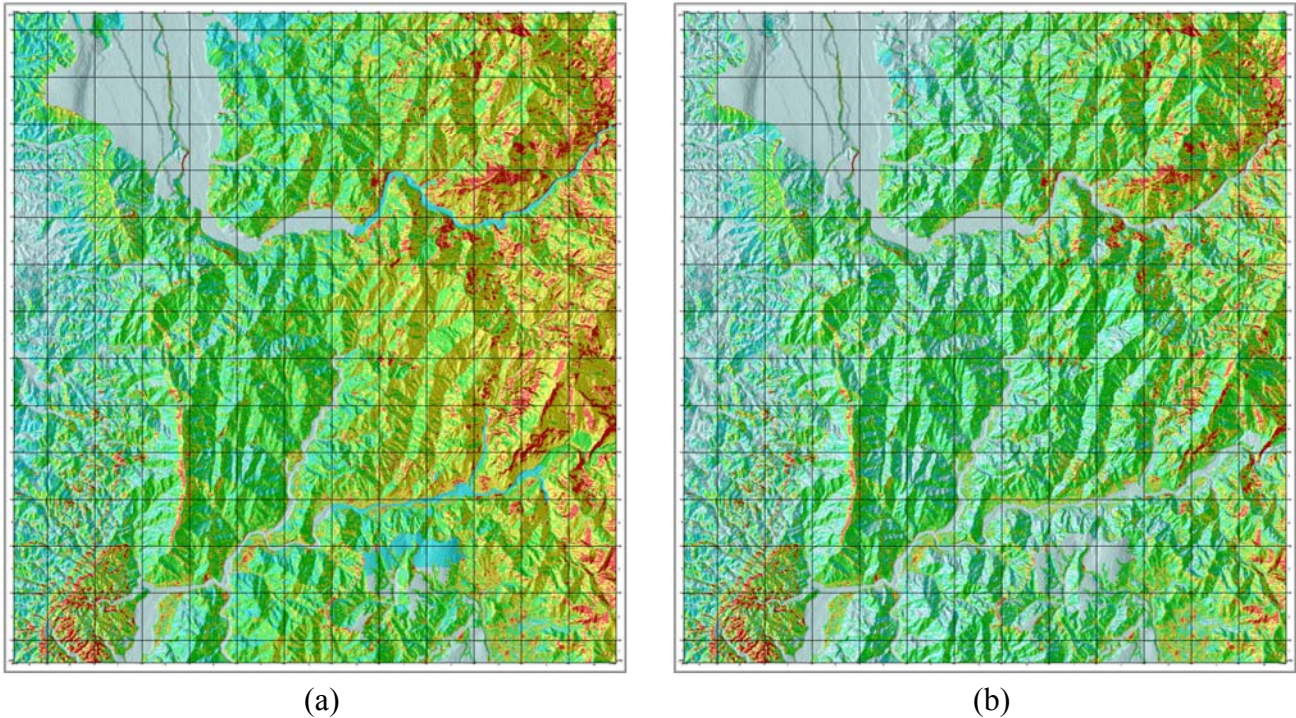


Fig. 9 Landslide susceptibility maps of the Toraji event. Red indicates high susceptibility, yellow moderately high, green moderate. (a) The Toraji event, (b) pre-Toraji event.

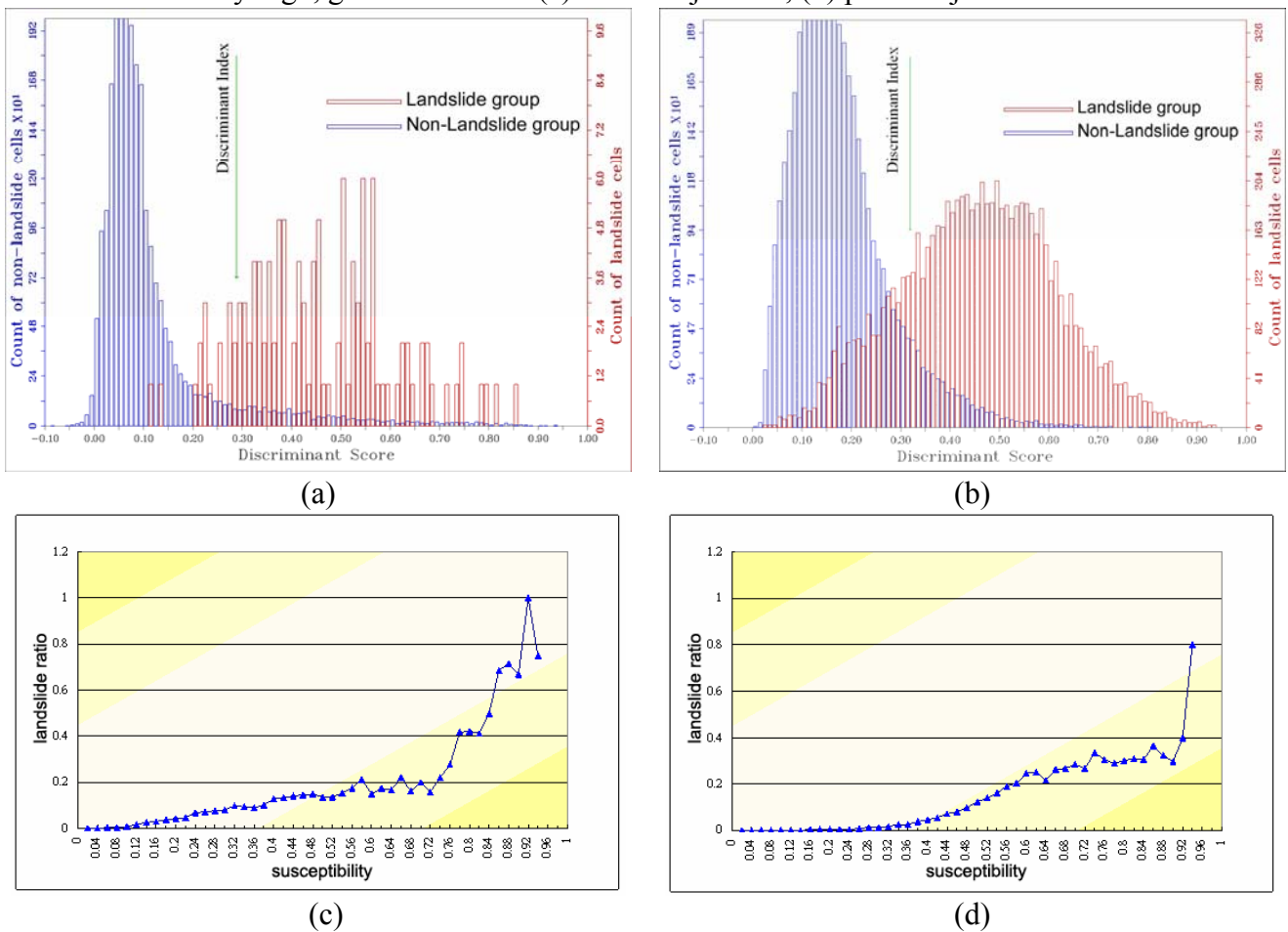


Fig. 10 Frequency distribution of discriminant score in (a) hilly terrain and (b) mountainous terrain, and landslide ratio distribution of susceptibility value in (c) hilly terrain and (d) mountainous terrain.

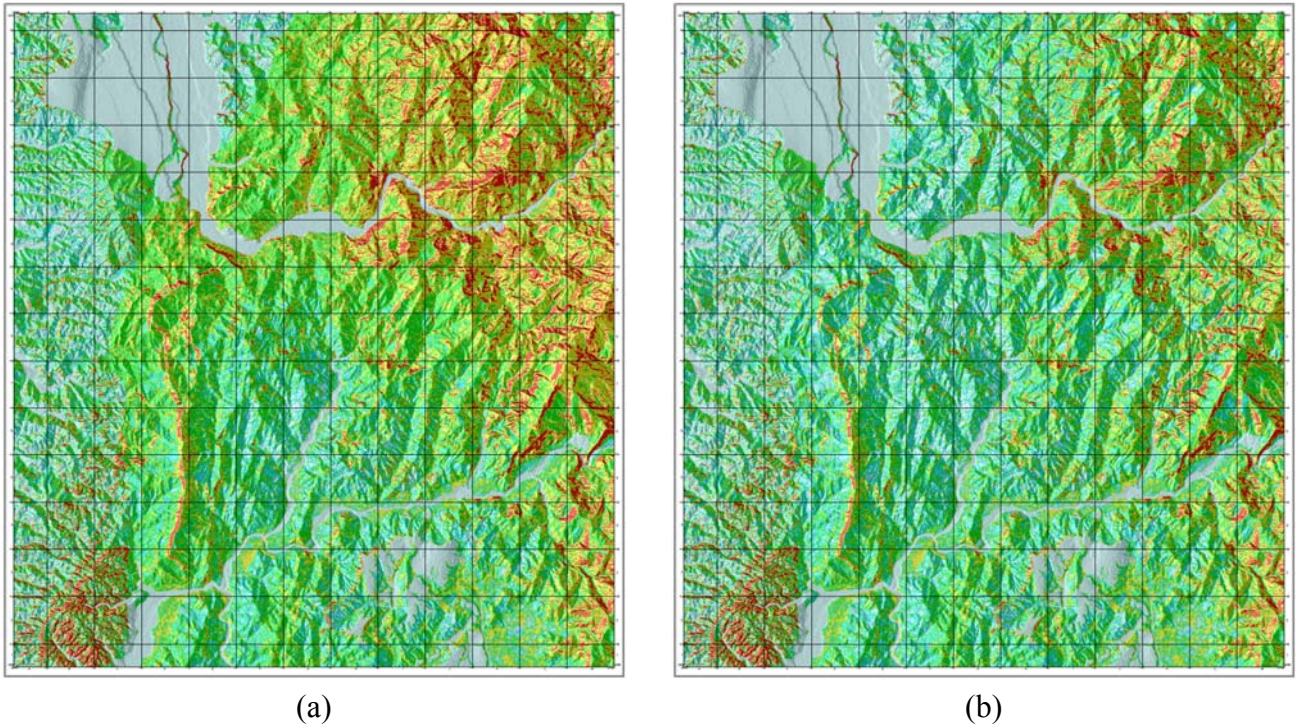


Fig. 11 Landslide susceptibility maps of the Herb event. Red indicates high susceptibility, yellow moderately high, green moderate. (a) The Herb event, (b) pre-Herb event.

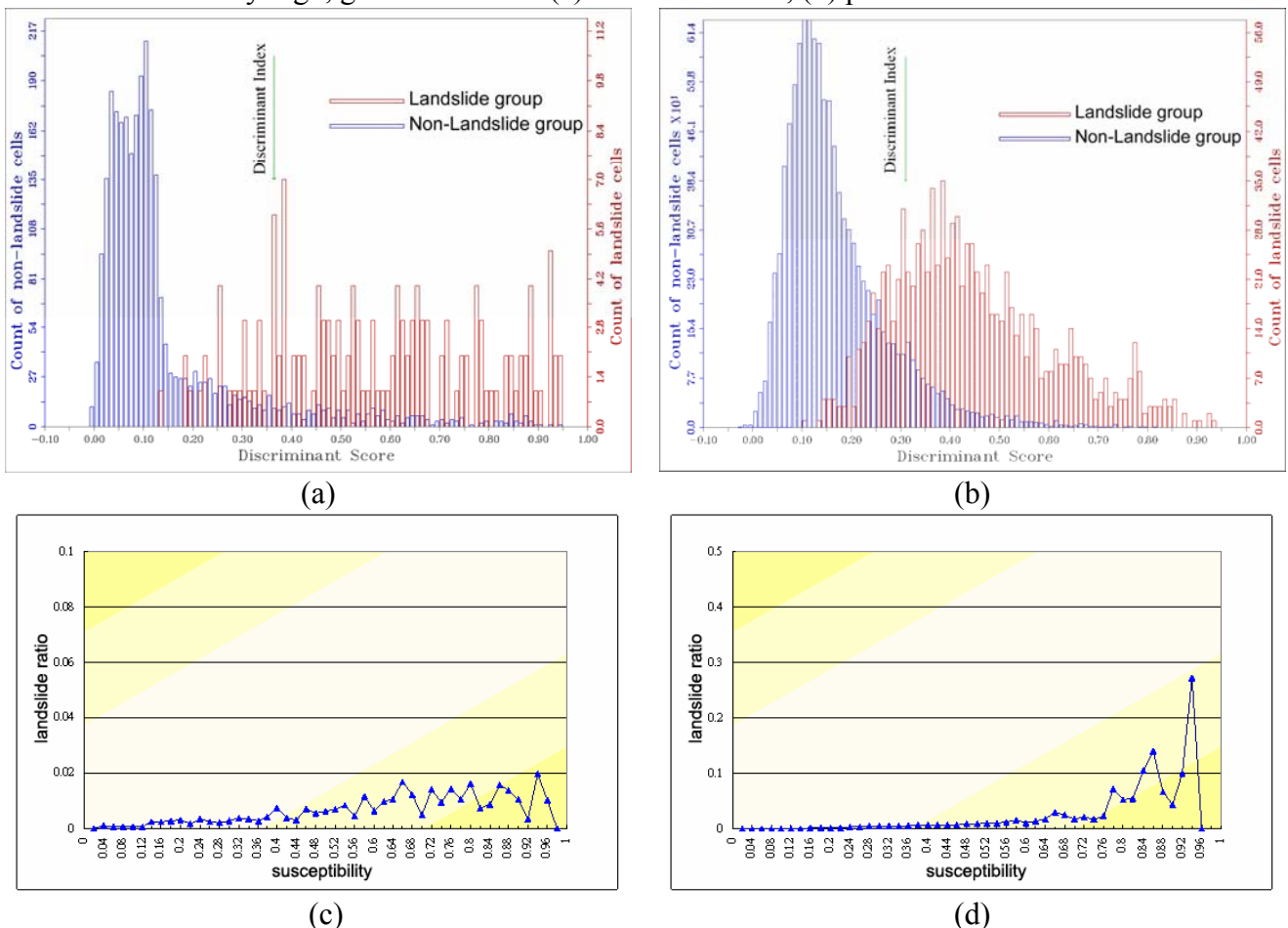


Fig. 12 Frequency distribution of discriminant score in (a) hilly terrain and (b) mountainous terrain, and landslide ratio distribution of susceptibility value in (c) hilly terrain and (d) mountainous terrain.

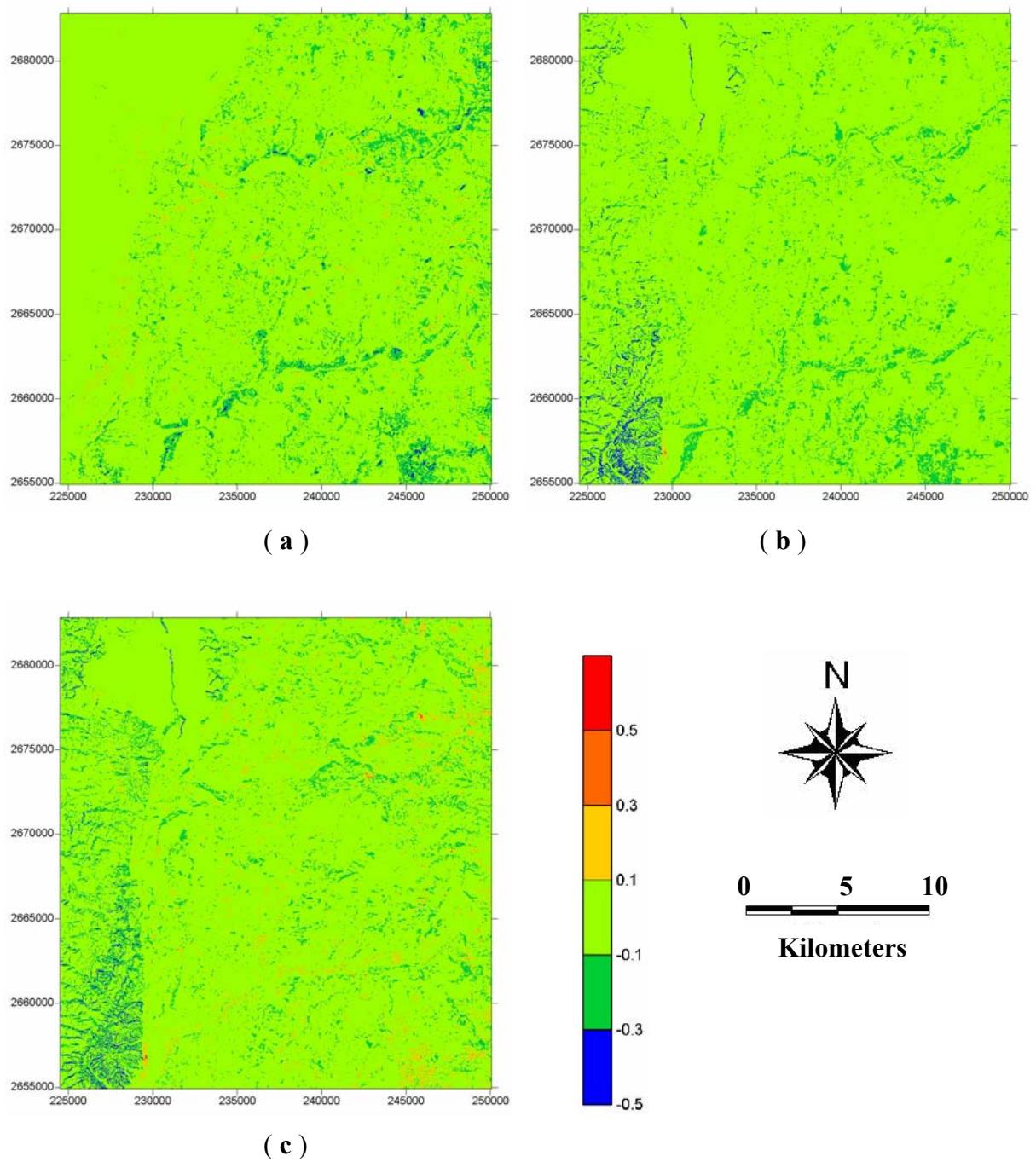


Fig. 13 Comparison of no-triggering factor landslide susceptibility maps between two events. (a) Pre-Chi-Chi map subtracted by pre-Toraji map, (b) pre-Chi-Chi map subtracted by pre-Herb map, (c) pre-Toraji map subtracted by pre-Herb map.